THE JOURNAL OF PHYSICAL CHEMISTRY C

pubs.acs.org/JPCC Article

Toward High-Precision Control of Transformation Characteristics in VO_2 through Dopant Modulation of Hysteresis

Aliya Yano, Heidi Clarke, Diane G. Sellers, Erick J. Braham, Theodore E. G. Alivio, Sarbajit Banerjee, and Patrick J. Shamberger*

Cite This: *J. Phys. Chem. C* 2020, 124, 21223–21231 Read Online

ACCESS | Metrics & More | Article Recommendations | Supporting Information

ABSTRACT: Metal–insulator transition materials such as VO_2 have garnered much attention in the field of neuromorphic devices because of their nonlinear behavior and orders of magnitude scale property changes. Of interest is the ability to control their transformation and hysteresis through dopants. However, a deep understanding of the effect of each dopant on the VO_2 system remains lacking. Here, we utilize an optical technique to investigate the changes produced by substitutional tungsten and interstitial boron dopants when compared to an undoped VO_2 system. Tungsten demonstrates the ability to decrease the transition temperature, reduce hysteresis, and increase the transformation width. Boron also shows small increases to the transformation width but is accompanied by a larger hysteresis and unique relaxation effects. Single-particle imaging demonstrates that broader hysteresis observed in ensemble calorimetry measurements results from variations of dopant incorporation among populations of particles. Additionally, both dopants seem to negate the size effects observed in undoped particles because of their ability to enhance or suppress point defect concentrations and thereby improve the consistency of hysteresis. Both effects are essential for utilizing VO_2 in practical applications such as neuromorphic devices requiring precise control of transformation characteristics.

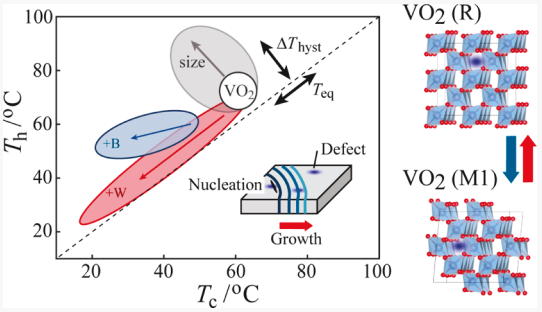

1. INTRODUCTION

There is a two-fold interest in chemical control of the coupled electronic structural transformation in strongly correlated oxide systems. The first is a fundamental approach to the role chemical dopants play in stabilizing different crystal structures and altering electronic band structure. The second is a practical need to tune the critical transformation temperature and the degree of volatility of the transformation.[1] Chemical doping has shown dramatic effects in changing the thermodynamic stability of various doped VO_2 phases, including promoting or depressing phase transformations by up to ~20 °C[2−6] and stabilizing phases that are not typically observed in undoped VO_2 upon simple heating and cooling.[7−9] However, while the effects of chemical dopants on general transformation behavior such as transition temperature have been explored, much still needs to be clarified about how these inclusions change the mechanisms of the transformation such as hysteresis, nucleation, and growth. Doping could modify the behavior of the electronic structural phase transformation through at least three mechanisms: (1) by altering the energy landscape of the system, including the magnitude of energy barriers limiting forward and reverse transformation,[10] (2) by stabilizing intermediate phases, which may introduce alternative transformation paths, or (3) by introducing localized regions of strain surrounding chemical dopants, which could affect local thermodynamic equilibria heterogeneously throughout a sample. Importantly, all three mechanisms could impact either energy barriers, limiting nucleation of a new daughter phase within a parent phase, or the mobility of heterophase boundaries and consequently the rate of domain growth of a daughter phase. Identifying changes in phase transformation mechanisms requires microscopic investigation of domain nucleation and growth. In studying this system, we can expose underlying clues to understand transformation mechanisms in both undoped and chemically doped systems. These further reveal new approaches to engineering metal–insulator transitions (MITs) with desired transformation behavior.

VO_2 exhibits a coupled electronic structural transformation which results in significant changes to properties, including a 4 order of magnitude increase in electrical conductivity,[11,12] nearly 1 order of magnitude decrease in infrared transmittance,[13,14] and a 60% increase in thermal conductivity.[15,16]

Received: June 1, 2020
Revised: September 4, 2020
Published: September 4, 2020

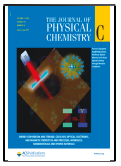

https://dx.doi.org/10.1021/acs.jpcc.0c04952
J. Phys. Chem. C 2020, 124, 21223–21231

At low temperatures, VO_2 crystallizes in an insulating, monoclinic (M1) phase with space group $P2_1/c$. Upon heating to ~67 °C, it transitions to a metallic, higher symmetry rutile phase (R) with space group ($P4_2/mnm$).[17] However, because of its strong electron−phonon correlation, it is difficult to determine the origins of the MIT.[17] This subject has generated much debate as VO_2 exhibits aspects of electron screening seen in Mott−Hubbard transitions[11,18] as well as dimerization of V−V bonds and subsequent opening of the band gap that is often associated with Peierls transitions.[19−21]

VO_2 is most commonly studied as either freestanding particles—often grown through a hydrothermal process—or elastically clamped films or particles grown directly on a substrate.[7] The synthesis method can affect the residual stress state, which significantly affects the transformation behavior of VO_2. Elastically clamped VO_2 has a large amount of phase coexistence because of transformation-induced local strain.[22] Freestanding single-crystalline particles, in contrast, experience rapid transformation with little phase coexistence, possibly caused by its ability to deform easily and limited extended defects to impede domain growth.[23] These freestanding, undoped particles likely utilize different defects to nucleate phases on heating and cooling.[23,24] It should be noted that in addition to the M1 and R phases, studies have found that an alternative monoclinic phase (M2) of space group $C2/m$ can form under strain—for example, M2 is seen in both elastically clamped particles[7,8] and W-doped particles.[9] Additionally, a triple point has been measured at the transition temperature in undoped VO_2 nanobeams, which is subject to much study.[25]

In addition to being a method for stabilizing additional phases, dopants can modify transformation behavior through their impact on both the electronic and lattice structure of VO_2 as even slight discrepancies from the host lattice atoms can have large implications. These dopants can induce anisotropic strain in the lattice and cause variations of the band structure and therefore the Mott behavior.[26] Germanium[2] and titanium[3,4] are two examples of substitutional dopants known to increase the critical transformation temperature, while others such as molybdenum[5] and tungsten[27] cause a significant decrease. As dopants, germanium and titanium have the same oxidation state as vanadium—formally, 4+, while molybdenum and tungsten are found as nominally pentavalent and hexavalent.[5,27] While formal valence undoubtedly plays a role in the modification of transformation behavior, it is not solely responsible. For example, small interstitial dopants such as hydrogen or boron have also been introduced into the VO_2 structure to modify transformation behavior.[28,29] Interstitial dopants generally have smaller radii than their substitutional counterparts, which must be similar in size to the host atoms, yet both types are capable of engendering some degree of strain on the host lattice.[28,30,31] Hydrogen has a very small atomic radius and sits in interstitial tetrahedral sites within the VO_2 lattice.[28] This small inclusion has a large effect as a fully hydrogenated sample shows a 13% increase in volume and interferes with the Peierls dimerization that is characteristic of MITs. It also induces higher d-orbital occupancy in the vanadium and pushes the behavior away from Mott transitions. Therefore, increased hydrogen doping preferentially stabilizes the metallic rutile phase by making the Peierls and Mott behaviors unfavorable and erases the MIT entirely.[26] At significantly high concentrations, this metallization disappears and the insulating phase reemerges.[32] Boron also preferentially stabilizes the metallic phase, but unlike H, it does this by modifying the phase equilibrium temperature (decreasing critical temperature by *ca.* 10 °C/atom %)[28] rather than increasing metallicity in the insulating phase. In this way, it also retains MIT characteristics in highly doped samples.[28] Because of its small size, boron is also highly mobile within the VO_2 lattice, which results in unique, time-dependent behavior. As the VO_2 host lattice quickly switches between R and M1, the boron is trapped in a metastable site from wherein it relaxes back into its M1 site.[33]

Microscopic characterization of thin films and freestanding particles is necessary to better understand domain nucleation and growth. This has been accomplished by utilizing different aspects of the phase change. For example, X-ray holography, capable of resolving domains at least 50 nm in diameter, has shown that metallic domains nucleate at and span between nanoscale defects at grain boundaries in VO_2 films.[22] With finer temperature resolution, this method was able to identify the evolution of individual phases (M1, M2, and R) through the MIT. Asayesh-Ardakani *et al.* used *in situ* TEM to monitor the transformation of highly W-doped (0.8 at % W) single-crystal nanowires and were able to corroborate the existence of M1, M2, and R phases of VO_2 through the transition, even without epitaxial strain due to lattice effects.[9,34] Other techniques such as atomic force microscopy, Raman, and s-SNOM,[35] are also capable of observing microscopic domain evolution, but they are spatially and temporally cost-limited. A more efficient, albeit lower-resolution, method takes advantage of the slight change in reflectance that VO_2 exhibits as it transitions from M1 to R.[23] With this method, Clarke *et al.* collected data such as transformation temperature, hysteresis, and width of transformation on an ensemble of ~300 undoped VO_2 freestanding particles and determined that size plays a key role in transformation behavior. Statistically, as particle size increases, so do the number of available nucleation site defects, which leads to decreased hysteresis. Additionally, transformation temperature on heating and cooling was uncorrelated, suggesting that different nucleation points contribute to each transformation.

In this paper, we utilize optical microscopy to collect data on individual particles of doped VO_2 in order to explore how dopants fundamentally alter transformation behavior. Using this method, we uncover trends from aggregate population data as well as identify transformation mechanisms within a particle. Undoped VO_2 particles are held as the control, while W and B dopant systems are investigated as a canonical example of interstitial and substitutional dopants, respectively. We show that each dopant has unique effects from increasing transformation width, suppressing hysteresis and changing transformation temperature. Understanding the underlying mechanism of and demonstrating tuning of the MIT behavior in VO_2 with dopants provides fundamental design rules for modulating an archetypal strongly correlated oxide system and allows VO_2 to be used more readily in a wider variety of electronic devices.

2. METHODS

2.1. Synthesis of Doped and Undoped VO_2. Doped and undoped VO_2 particles were synthesized hydrothermally from bulk V_2O_5 powder supplied by Beantown Chemicals, a reducing agent of anhydrous oxalic acid ($H_2C_2O_4$), acetone/isopropanol, dopant precursors of tungstic acid (H_2WO_4), and 2-allyl-4,4,5,5-tetramethyl-1,3,2-dioxaborolane (97%) from Sigma-Aldrich. Undoped particles were prepared with 1.63 g

https://dx.doi.org/10.1021/acs.jpcc.0c04952
J. Phys. Chem. C 2020, 124, 21223−21231

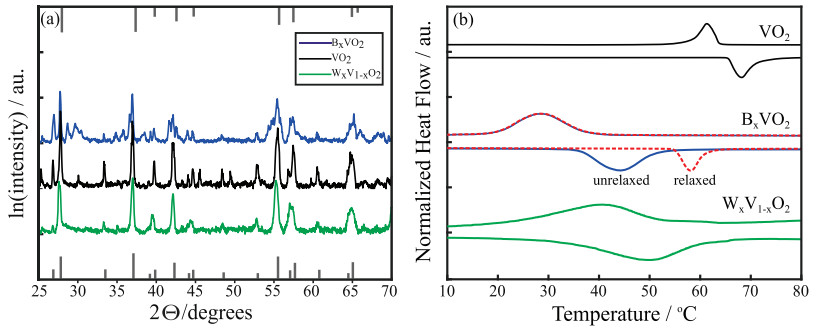

Figure 1. (a) XRD patterns of undoped (black), $B_{0.017}VO_2$ (blue), and $W_{0.007}V_{0.993}O_2$ (green) samples. Reflections corresponding to the M1 phase of VO_2 are plotted on the lower horizontal axis, whereas reflections corresponding to the R phase of VO_2 are plotted on the upper axis. (b) Normalized DSC traces with a ramp rate of 5 °C/min are given for undoped (black), $W_{0.0035}V_{0.9965}O_2$ (green), and for a $B_{0.021}VO_2$ sample, which was relaxed for a period of 323 days (red) at room temperature as compared with an unrelaxed cycle (blue) of the same sample. This relaxation effect is discussed further below.

of V_2O_5, 10 mL of isopropanol, and 65 mL of deionized water. Tungsten-doped samples were made with 300 mg of V_2O_5, 450 mg of $H_2C_2O_4$, and levels of dopant precursor necessary to obtain the desired concentration, which was then mixed with 15 mL of deionized water. Both undoped and W-doped mixtures were placed in 125 and 23 mL polytetrafluoroethylene cups and heated in a high-pressure autoclave reactor at 210 and 250 °C, respectively, for 72 h. Samples were recovered through vacuum filtration and washed three times with deionized water and acetone. Finally, the samples were annealed under Ar (g) at 550 °C for 5 h to relieve any strain that may occur from synthesis.[36]

Boron dopants were incorporated by dispersing 20 mg of undoped VO_2 particles in 1.00 mL of mesitylene by ultrasonication and adding 200 μL of 2-allyl-4,4,5,5-tetramethyl-1,3,2-dioxaborolane to the reaction mixture. This mixture was stirred for 2.5 h at 120 °C under ambient Ar (g) in a Schlenk flask. The particles were recovered by centrifugation, rinsed with toluene, and annealed in a 2 mL porcelain combustion boat (VWR, Sugar Land, TX) at 900−950 °C for 1 min under ambient Ar (g) in a quartz tube furnace. The final samples were nanowire structures with uniform heights and varying lengths and widths.[28]

2.2. Differential Scanning Calorimetry. Differential scanning calorimetry (TA Instruments, Q2000) was conducted on ∼10 mg of doped and undoped powders at 5 °C/min to verify the occurrence of a transformation and to determine the temperature range of the transition of the powder sample. DSC measurements are calibrated using an indium enthalpy standard and has a temperature accuracy of ±0.1 °C.

2.3. Optical Microscopy. In order to conduct optical microscopy studies, the samples were first dispersed by sonication in high-purity ethanol. A drop of the suspended VO_2 particles was then placed on a glass coverslip and ethanol was allowed to evaporate, leaving only the particles on the glass slide. Particles were further mechanically redistributed by passing another coverslip over the surface of the sample. Particles were loosely adhered to the glass substrate through weak secondary bonding, resulting in negligible strain unlike that when clamping or grown on a substrate.

Optical microscopy was performed with an Olympus BX-53 polarized light microscope and images were captured on an Olympus UC30 color CCD camera. All images were collected under bright-field-reflected unpolarized white light. With these conditions, a clear blue shift in the reflected light can be observed as the VO_2 particle transition from the low-temperature monoclinic phase (M1) to their high-temperature rutile phase (R) as there is a decrease in reflectivity between 600 and 800 nm in the R phase.[37] Exposure was manually selected and sustained through the image series. Temperature was controlled with a Linkham LTS120 Peltier temperature stage with a range of −25−120 °C with an accuracy of ±0.1 °C.

3. RESULTS AND DISCUSSION

3.1. Phase Equilibria in Doped VO_2 Systems. *3.1.1. Structural Characterization.* A combination of X-ray diffraction (XRD) and DSC was used to evaluate both M1/R phase structure and equilibria (Figure 1), revealing that equilibrium transformation temperatures were depressed with both W and B dopant incorporation. XRD characterization showed predominantly M1 phase present for undoped VO_2 at room temperature (Figure 1a). Previous studies have shown that slight broadening of selected reflections in the XRD patterns of W-doped VO_2 implies changes in lattice spacing[36] because of W inclusion causing anisotropic lattice expansion in the M1 phase, concurrent with the findings of anisotropic strain in XAFS studies.[30] These structural distortions accompany a decrease in phase transition temperatures such that a predominantly monoclinic phase was obtained at room temperatures only in low dopant concentration samples (Figure 1a). In contrast, B dopant inclusion in interstitial lattice sites has been shown to cause very little change in the lattice parameters,[28] although at room temperature, a mix of the M1 and R lattice reflections is realized as a result of phase coexistence in this temperature regime (Figure 1). Small amounts of impurity phases, including V_6O_{13} and V_8O_{15}, are identified in undoped and B-doped samples, respectively, as a result of aging in atmosphere in the former case and increased VO_2 reduction during high-temperature annealing in the latter. Although these compounds do undergo MITs, V_6O_{13} undergoes its phase transition at 423 °C,[38] while V_8O_{15} undergoes an MIT at −203 °C.[19] With both critical temperatures being far outside the range sampled here, their impact on these results is minimal.

3.1.2. Bulk Transformation Behavior. DSC characterization demonstrates depression of transition temperatures upon W and B doping, accompanied by broadening of transformation peaks. The peak maxima of DSC traces were taken as critical transition temperatures, and both heating (T_h^{pk} ∼68 °C) and

https://dx.doi.org/10.1021/acs.jpcc.0c04952
J. Phys. Chem. C 2020, 124, 21223−21231

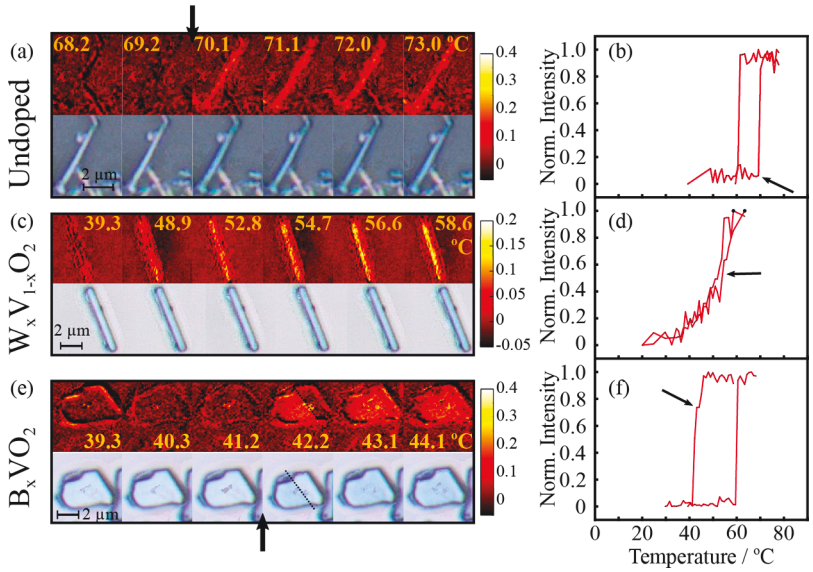

Figure 2. Optical bright-field reflected unpolarized white light images of individual particles, accompanied by extracted cumulative differences in red intensity between base image and images as a function of temperature for (a) undoped particle, (c) $W_xV_{1-x}O_2$ particle, and (e) B_xVO_2 particle. Normalized cumulative difference for area sums of red pixel intensity for outlined particles between a reference image taken at a base temperature and images at increasing temperature (1 °C increments) are used to track the phase fraction transformed for representative (b) undoped particles, (d) $W_xV_{1-x}O_2$ particles showing a variety of transition width symmetries, and (f) B_xVO_2 particles. The black arrows in (a,e) indicate the temperature step over which the phase transformation occurs; in (b,d,f), they serve to illustrate the different transformation types of one-step, gradual, and multistep.

cooling (T_c^{pk} ~62 °C) values obtained in undoped samples align with widely accepted transition values.[11] The integrated peak enthalpy (57.7 J/g) is comparable to that reported by Cook *et al.* (52.45 J/g),[20] confirming phase purity and expected transformation behavior in undoped wire VO_2 samples (Figure 1b). Transition temperatures as measured by DSC were correlated with concentrations determined by XPS and inductively coupled plasma optical emission spectroscopy (ICP-OES) for the specific materials used in this study.[28,39] Boron and tungsten dopants display a nearly linear relationship between the concentration of dopant and transition temperature with −10−15 and −48−56 C/atom %, respectively.[28] It should be noted that other sample morphologies display different relationships, with tungsten thin films showing −10−27.8 C/atom % while nanobeams contain −18.4 C/atom %.[40,41] Additionally, theoretical studies of both dopant systems also predicted slightly different relationships of −18.6−27 C/atom % of W and 79−83 C/atom %.[31,42] Though magnitudes of these relationships differentiate, all are still nearly linearly decreasing. Four separate W_xVO_2 samples were utilized in this study, with $0.0003 < x < 0.0035$, based on the calibration of T_c^{pk} with W dopant concentration measured by ICP-OES (52 °C/at % W).[39] Within individual $W_xV_{1-x}O_2$ samples, broad peaks were observed with a maximum width of 30 °C measured between peak onset and peak finish (Figure 1b), indicating either a wide variation in incorporated dopant concentration between particles or wide span of the phase transition within individual particles. A single nominal concentration of boron was utilized for this study, $B_{0.017}VO_2$, calculated using the calibration (15 °C T_c^{pk}/at % and T_c^{pk} = 35.46 °C) as measured by XPS.[28] As in the case of W doping, B dopant concentration led to relatively broad peaks upon heating and cooling (35 °C), indicating a range of dopant concentration incorporation or larger range of phase coexistence in individual particles. Single nanoparticle imaging studies described below are able to differentiate between these two possible origins of the broad DSC peaks. It is essential to note that cycling and time-dependent effects were observed in B-doped samples. A particle that has not previously been switched (relaxed) displays different transformation behavior than one that has recently undergone a phase (unrelaxed). Therefore, the relaxed or unrelaxed state of the sample is important for understanding the behavior.

Moreover, W and B dopants introduced varying degrees of peak transformation temperature dependence on the DSC scan rate, which contributes to hysteresis measured at fast ramp rates (>1 °C/min). In undoped VO_2, both T_c^{pk} and T_h^{pk} symmetrically increased as a function of increasing scan rate (Figure S1). This kinetic dependence has previously been explained by the Arrhenian nature of rate-limiting nucleation barriers between the M1 and R phases.[23] As the ramp rate increases, there is less time allowed for the high energy nucleation points to be activated. Therefore, they trigger at larger degrees of supercooling or superheating.[36] W-doped samples, however, show no significant dependence on the ramp rate for T_c^{pk} or T_h^{pk}. This ramp rate independence is likely due to different, more potent, nucleation points being utilized in the W-doped case.[36]

The ramp rate dependence of B-doped VO_2 transition temperatures shows strong deviations from both undoped and W-doped effects. Following a relaxation period of 2 weeks, a 12 °C increase in heating transition temperature (T_h^{pk}) was observed in a $B_{0.02}VO_2$ sample (near the x = 0.017 concentration observed in this study), with no change occurring in the critical cooling transition peak temperature (Figure 1b). Moreover, a significant reduction of the width of the heating transformation peak (24−12 °C) is observed with increased relaxation time, indicating a narrowing of the distribution of equilibrium transformation temperatures either within or between particles. Thus, thermal profiles allowing for

https://dx.doi.org/10.1021/acs.jpcc.0c04952
J. Phys. Chem. C 2020, 124, 21223−21231

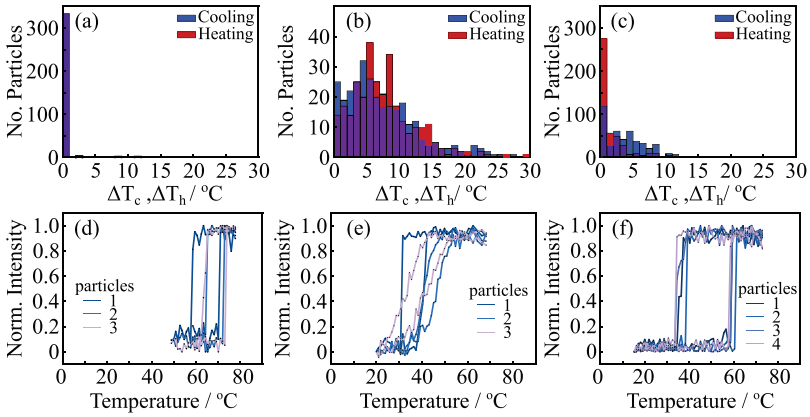

Figure 3. Histograms of the span of heating (red) and cooling (blue) transition widths (ΔT_c and ΔT_h) are given for (a) undoped particles, (b) $W_xV_{1-x}O_2$ particles, and (c) B_xVO_2 particles. Representative hysteresis loops of selected particles for (d) undoped particles, (e) $W_xV_{1-x}O_2$ particles, and (f) B_xVO_2 particles.

longer periods of time spent below the M1 to R transition temperature showed increased values of T_h^{pk} as well as narrowing of the transformation peak. It should be noted that the DSC trace on unrelaxed particles shows similar broad transition peaks and depressed transformation temperatures as seen in Braham *et al.*[36]

Independent of ramp rate, hysteresis (measured from peak to peak $\Delta T_{hyst} = T_h^{pk} - T_c^{pk}$) is strongly impacted by the addition of W and B dopants when compared to that of undoped VO_2. ΔT_{hyst} is approximately 5−8 °C for undoped VO_2 (measured at 5 °C/min in all cases) but varies between 9.3 ± 0.3 to 3.0 ± 0.2 °C for $W_xV_{1-x}O_2$ samples as a function of increasing W dopant concentration (Figure S1c). Such a scaling has been previously observed and suggested to arise from an increased amount of tensile lattice strain, leading to increased degrees of phase coexistence as a function of dopant concentration,[43] whose individual particle basis is further explored in this work. In the limited range of B dopant concentrations studied here, the "unrelaxed" ΔT_{hyst} is independent of boron concentration and a uniformly greater magnitude hysteresis is observed compared with undoped samples, ∼14 °C (Figure S1c).

3.2. Phase Coexistence and Characteristic Domain Size. *3.2.1. Undoped VO_2 Particles.* As VO_2 undergoes the MIT around ∼68 °C, optical microscopy of the spatial distribution of R and M1 phases indicates that the phase transition in an ensemble of individual VO_2 wires (N = 347) occurs abruptly through the particle volume. The transition occurs at a range of temperatures between individual particles (Figures 2, 3), which is consistent with nucleation-limited transformation behavior. Phase coexistence in this case is only observed in ∼4% of particles in which the phase front is likely pinned by a microscopic defect, occurring in a maximum of two temperature increments. Within 2 degrees, all the particles transform completely. Using the intensity of reflected red light as an indicator of the phase present in a particular area, hysteresis loops indicating the extent of the transitions at a particular temperature can be extracted (Figure 1). $T_c^{0.25}$, $T_c^{0.5}$, and $T_c^{0.75}$ are defined as the temperature corresponding to a volume fraction of 0.25, 0.5, and 0.75 of the individual particles having transformed on cooling, respectively ($T_h^{0.25}$, $T_h^{0.5}$, and $T_h^{0.75}$ represent the same for the case of heating). Thus, $T_c^{0.25}$ is a proxy for the "start" of the transformation on cooling, while $T_c^{0.75}$ is a proxy for the "end" of the transformation. Extracted hysteresis loops and calculated transformations widths on cooling, ΔT_c, and heating, ΔT_h (where $\Delta T_c = |T_c^{0.75} - T_c^{0.25}|$) show that the transformation behavior is symmetric and sharp upon heating and cooling within individual particles (Figure 3). Such nucleation-limited, symmetric behavior mirrors phase transition behavior observed in freestanding, undoped VO_2 widely reported in other studies on single-crystal particles.[7,35,44,45]

3.2.2. $W_xV_{1-x}O_2$ Particles. In contrast to phase transformations in undoped VO_2, transformations in W-doped VO_2 generally show gradual transformation over multiple temperature intervals with no domains that are distinguishable on the length scale of optical observations in most particles. Clearly defined abrupt transitions with characteristic domains on the order of a few microns are observed in only ∼0.1% of the particles imaged. The phase transition in W-doped VO_2 shows a slightly smaller change in red intensity (between 15 and 90 °C) than undoped VO_2 (Figure 1), which is nevertheless distinct in reflected unpolarized white light (Figure S2). Precise start and finish temperatures are difficult to clearly define because of the gradational nature of the transformation. $T_c^{0.25}$, $T_c^{0.5}$, and $T_c^{0.75}$ are calculated from hysteresis loops for individual particles by isolating the specific area associated with a single particle. The progression of the phase transformation could then be evaluated by monitoring the integrated intensity of reflected light (Figure 2). Although optical observations are unable to discern clear domains of low-temperature (M1) and high-temperature (R) phases, the gradational nature of the transition is consistent with characteristic domain length scales in submicron regimes, smaller than discernible by optical microscopy. This claim is supported by high-resolution TEM observations of W-doped hydrothermal VO_2 particles, which illustrate phase coexistence on length scales <10 nm.[9] Furthermore, TEM observations suggest the existence of the M2 phase at the interface between M1 and R phases, which is also not observable at optical length scales.[9]

Establishment of a distribution of local equilibria between nanoscale M1, R, and M2 domains is considered to be caused by inhomogeneous strain fields around W dopants.[36] Other than direct TEM evidence of M1, R, and M2 domains, several other considerations support this picture. Shifting of reflections to lower 2θ values and broadening of peaks is observed in XRD of samples with bulk W dopant concentrations greater than 0.5 at %,[36] which indicates that W atoms introduce anisotropic

https://dx.doi.org/10.1021/acs.jpcc.0c04952
J. Phys. Chem. C 2020, 124, 21223−21231

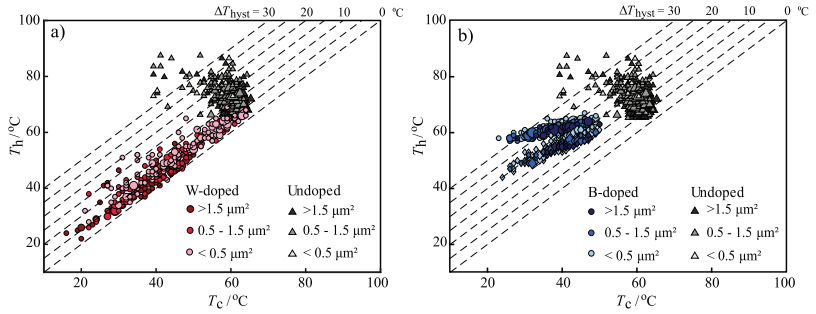

Figure 4. $T_c^{0.5}$ and $T_h^{0.5}$ temperatures of transitions in individual particles demonstrating hysteresis trends binned by particle area for (a) W-doped (N = 305) and undoped VO_2 particles (N = 347) and (b) B-doped (N = 375) and undoped VO_2 particles (N = 347). Iso-hysteresis lines are represented by dashed black lines. Diamonds signify unrelaxed BVO_2 particles and the size of the markers represents how many particles lie at that data point.

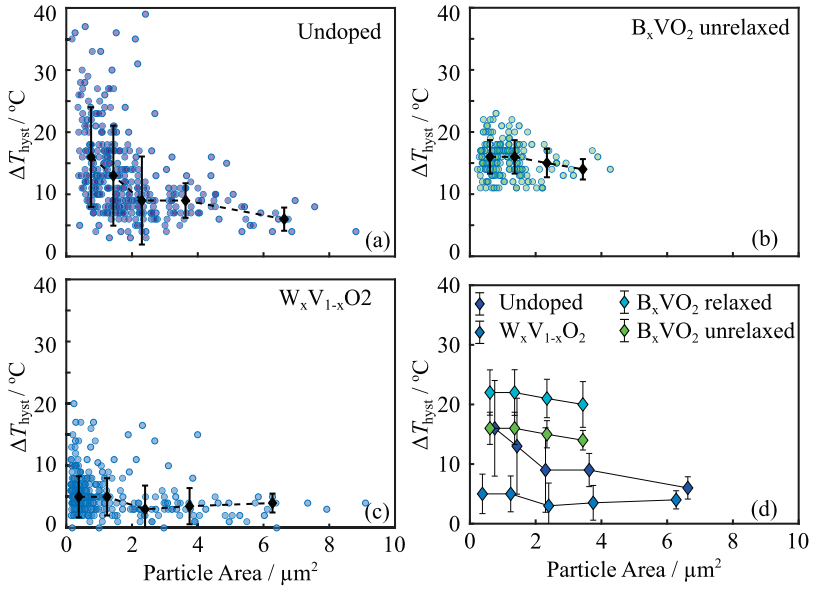

Figure 5. Scaling of hysteresis width as a function of particle area (a) undoped, (b) B_xVO_2, and (c) W_xVO_2 particles. Particle areas are binned with black diamonds to denote their median hysteresis.

expansion of the lattice. Moreover, it has been previously shown that the larger ionic radius of the W atoms as compared to V structurally distorts the monoclinic lattice toward a more tetragonal-like symmetry, accompanied by increased interatomic separation of V−V bonds,[30] which serves to alter electronic band overlap and phase equilibria. Although lattice strain is not resolved in samples with 0.03−0.32 at % W, inhomogeneous lattice strain could lie beneath refinement limitations of XRD analysis. For instance, the highest W concentration considered here (0.32 at %) would correspond to a W spacing of ∼80 nm, on the same order as the domain length scale, while the lowest concentration (0.07 at %) would still yield a spacing of ∼350 nm between W dopants. Although TEM imaging suggests a homogeneous distribution of W atoms throughout the sampled volume,[9,36] it is unknown whether defect clusters of W atoms form and it is likely that the resultant stress fields are neither uniform nor constant, so that the pattern of domains distributed throughout the particle is an irregular patchwork defined by the multiphysics coupling of dopant localization with surface stresses and particle dimensions/morphology.

The majority of particles sampled show a range of symmetric transformation widths including sharp transitions (ΔT_c, ΔT_h < 5 °C) both on heating and cooling (35%) as well as gradual transitions during both heating and cooling (43%). However, there is a distinguishable asymmetry between heating and cooling cycles in the transition width for a significant proportion of sampled particles (22%). Of these, approximately 65% demonstrate a wide heating transition (ΔT_h > 5 °C), while the corresponding cooling transition is sharp (ΔT_c < 5 °C; Figure 2). Such transformation asymmetry could stem from asymmetric nucleation or growth barriers between heating and cooling as might be expected from different defect populations serving as the potent nucleation sites. The presence of separate nucleating defects has been demonstrated in clamped VO_2 wires, where point defects serve to nucleate the cooling transition, while higher energy (more potent) M1 twin boundaries serve as nucleation sites for the monoclinic to rutile transition.[24] By extension, Braham *et al.* have observed kinetic ramp rate dependence of T_c^{pk} and a lack of dependence of heating transition temperatures on ramp rate in bulk transformation of $W_xV_{1-x}O_2$ samples ($0.21 < x < 0.32$ at. %). These data are consistent with nucleation at point defects during cooling and at M1 twins or M1/M2 phase boundaries on heating.[36] The range in transformation behaviors suggests that in individual particles, different nucleation or growth

https://dx.doi.org/10.1021/acs.jpcc.0c04952
J. Phys. Chem. C 2020, 124, 21223−21231

pathways are at work whether that be due to intrinsic defects, dopants, or strain.

3.2.3. B_xVO_2 Particles. Observations of phase transitions in an ensemble of individual B_xVO_2 particles ($N = 399$) show that transitions are relatively sharp with clear phase coexistence boundaries discernible at optical length scales. The characteristic domain length scales are on the order of 1.0 ± 0.7 μm^2. Extracted hysteresis loops also show distinct steps over 1 °C increments on cooling, in stark contrast to the gradual transformations introduced by W dopants (Figures 2 and 3). Such micrometer scaling of domain length scales is observed despite an equivalent dopant concentration as used in W-doped samples, with expected B concentration (1.7 at %) yielding a spacing of ∼10 nm. Such a result is consistent with the small ionic radius of B in an interstitial site, which adds minimal distortion to the lattice and the V−V spacing.[28] Therefore, although B is present in high concentrations, inhomogeneous lattice strain gradients are not formed as in the case of W dopant addition, and nanometer scale domains are not stabilized.

The relatively sharp transitions with large extent of phase transition at each step observed in these particles point to a nucleation-limited phase transition. For the majority of particles, both ΔT_c and ΔT_h are <1 °C. Therefore, DSC observations of wide heating and cooling peaks (∼20 °C) are associated with the chemical equilibria distributed between particles as a result of uneven dopant incorporation, rather than the span of a transition within a single particle (ΔT_c, ΔT_h < 10 °C). However, a limited degree of pinning occurs, and an asymmetry between heating and cooling transitions is observed in boron-doped particles. For the heating transition, 80% of particles transition with ΔT_h < 1 °C. During the cooling transition, only ∼30% of particles transition with ΔT_c < 1 °C, with a median ΔT_c of 2 °C. As in the case of $W_xV_{1-x}O_2$, this asymmetry could stem from differences in nucleation or growth barriers between heating and cooling.

3.3. Effects of Dopants on Transformation Hysteresis.

3.3.1. Undoped VO_2 Particles. Hysteresis was measured in individual particles as $\Delta T_{hyst} = T_h^{0.5} - T_c^{0.5}$. Undoped particles demonstrate a wide range of hysteresis from about 5° to more than 40 (Figure 4). Most notably, hysteresis in undoped VO_2 is dependent on particle size. $T_h^{0.5}$, $T_c^{0.5}$, and ΔT_{hyst} scale strongly and symmetrically with particle size, with particles <1 μm^2 experiencing ΔT_{hyst} up to 40 °C, and with particles larger than 2 μm^2 having an average ΔT_{hyst} of 8 °C (Figure 5). This observed particle size scaling in hydrothermal VO_2 wires has previously been explained using statistical models developed for observation of nucleation-limited transformation in martensitic Fe−Ni alloy small particle experiments.[23,46,47] The model assumes that defects that serve as potent nucleation sites are sparsely dispersed throughout the volume. Therefore, larger particles contain more potent sites than small particles and are more likely to undergo phase transformation near equilibrium. Because symmetric particle size scaling is observed between heating and cooling transitions, the presence of separate nucleating point defect populations cannot be supported. Fitting of collected transformation data for an ensemble of hydrothermal undoped VO_2 particles to this model resulted in a calculated potent nucleation site density ∼10^{13} cm^3,[11,23] which agrees with the qualitative picture of sparse, noninteracting potent nucleation sites.

3.3.2. $W_xV_{1-x}O_2$ Particles. Introducing W into the VO_2 particles dramatically decreases the transformation hysteresis within a particular particle, while simultaneously increasing the temperature range over which the aggregate transformation occurs (Figure 4). In 305 individual particles, all were at or below 20 degrees of hysteresis with a few (∼1%) showing zero hysteresis (Figure 4). This is a reduction of the range by more than half of that found in undoped VO_2 (45°). The concentration of W-dopant is seen to have no correlation with hysteresis, with highly and lightly doped particles performing within a few degrees of hysteresis (Figure S3). Additionally, particles that were lightly doped (∼0.02 at %) were able to retain transformation similar to those seen in undoped VO_2 while maintaining a lower hysteresis (Figure 4). The broad peaks observed with a maximum width of 30 °C measured between peak onset and peak finish in DSC measurements thus derive primarily from inhomogeneities in W incorporation across the ensemble of particles as well as an extended phase coexistence regime. However, the observed hysteresis in ensemble measurements relates primarily to variations in W-incorporation across populations of particles.

In comparison to undoped VO_2, hysteresis shows only weak correlation with particle area in $W_xV_{1-x}O_2$ particles ($R = 0.23$, $p = 0.001$, $\alpha = 0.05$; Figure 3). This lack of scaling of hysteresis in doped VO_2 with particle size is unsurprising in the context of extrinsic doping at high concentrations ∼10^{20} cm^3 *versus* intrinsic potent nucleation site densities ∼10^{13} cm^3 in undoped VO_2. Similarly, in monoclinic to tetragonal phase transitions in HfO_2 and ZrO_2, particle size scaling is suppressed upon the introduction of extrinsic defects, which serve as more potent and more readily available nucleation sites.[11,47,48] Therefore, by introducing point defects or W-dopants, the size dependence found in undoped VO_2 can be negated and supplanted by a dopant perturbation-mediated mechanism.

3.3.3. B_xVO_2 Particles. Overall, B_xVO_2 particles show an increased hysteresis when compared to $W_xV_{1-x}O_2$ particles, reaching a maximum of 35°, nearly equivalent to the bulk of undoped VO_2. Only the undoped particles experience a larger hysteresis. As in $W_xV_{1-x}O_2$, the hysteresis is significantly restricted to a range of 20° in the unrelaxed state. There are two distinct data sets (relaxed and unrelaxed) to consider in the case of B-doped particles. Fully relaxed particles are seen to have a hysteresis comparable to the highest found in the undoped case, ranging from 15 to 35°. Its unrelaxed state shows a slight decrease in hysteresis compared to its fully relaxed state (Figure 4). This decrease in hysteresis is especially evident in particles with larger dopant concentrations that subsequently transition at lower temperatures. Furthermore, in the fully relaxed particles, hysteresis is more dependent on dopant concentration as evidenced by the comparison in slopes. The smaller slope and nearly flat distribution of the fully relaxed data indicates that the hysteresis increases with increasing dopant concentration. The data for the unrelaxed particle exhibit a larger slope, closer to what is observed in the W-doped system and shows a uniform hysteresis for the full range of dopant concentrations. This behavior could be caused by simply inequal relaxation times and temperatures because of the cyclic nature of the data collection—particles with lower transformation temperatures had less time to relax than those at high temperatures.

Similar to $W_xV_{1-x}O_2$ particles, there is no correlation between hysteresis and area in B_x VO_2 particles. However, unlike in the W-doped case, overall hysteresis increases when B-dopants are introduced. This is despite the new, high concentration of point defects. As the B-dopants are relatively

https://dx.doi.org/10.1021/acs.jpcc.0c04952
J. Phys. Chem. C 2020, 124, 21223−21231

small, mobile, and reside in interstitial sites, there is no significant lattice strain caused by their inclusion.[28] Neither is there a large degree of phase coexistence observed as in the W case, which suggests that there is less pinning of domain boundaries occurring. The increase in hysteresis indicates that either (i) intrinsic nucleation sites (*e.g.*, oxygen vacancies, vacancy clusters, or dislocations) are scavenged by introduction of B dopants or (ii) the nucleation energy barriers are increased by B dopant introduction. Therefore, while B and W dopants suppress size effects in the hysteresis of VO_2 as expected from the introduction of extrinsic defects, the overall increase in hysteresis observed in B_xVO_2 samples is nontrivial. However, this explanation does not fully answer why the hysteresis range seen in B_xVO_2 particles is as restricted as that of $W_xV_{1-x}O_2$ (~20°). The tightening of hysteresis in $W_xV_{1-x}O_2$ particles is explained by W-dopants inducing potent nucleation sites, which is accompanied by an overall lowered hysteresis. Because B-doped particles do not have a reduced hysteresis, an alternate mechanism must exist. It is possible that instead of acting as nucleation sites, the B-dopant scavenges particular intrinsic defects, effectively reducing the range of nucleation while maintaining hysteresis comparable to undoped VO_2. The mobile nature of B atoms renders them amenable to transport to defect sites, wherein they can alter local distributions of point defects.

4. CONCLUSIONS

This work decisively shows that incorporating dopants can produce unique transformation behavior beyond simply modifying the transition temperature. W-doping enables a pinning effect that elongates the width of the transformation while still inducing potent nucleation sites that enable nearly zero hysteresis in the system. Alternatively, B-doping shows much smaller transformation widths, less phase coexistence, and maintains a relatively large hysteresis that is much more consistent than in the undoped case. Significantly, doping seems to also suppress size effects, enabling deterministic and reproducible control of hysteresis within dimensionally confined devices. Each of these findings contributes to the overall understanding of the VO_2 MIT behavior and informs further investigation into dopant effects. Given these observations, the incorporation of multiple dopants as a pathway to engineer particular attributes of the MIT transition remains an intriguing possibility, which will be investigated in future work.

■ ASSOCIATED CONTENT

Supporting Information

The Supporting Information is available free of charge at https://pubs.acs.org/doi/10.1021/acs.jpcc.0c04952.

Experimental data including rate-dependent DSC, additional optical microscopy images, and correlation plots between hysteresis and T_c and T_h (PDF)

■ AUTHOR INFORMATION

Corresponding Author

Patrick J. Shamberger − *Department of Materials Science, Texas A&M University, College Station 77843-3003, Texas, United States;* orcid.org/0000-0002-8737-6064; Phone: (979) 458-1086; Email: patrick.shamberger@tamu.edu

Authors

Aliya Yano − *Department of Materials Science, Texas A&M University, College Station 77843-3003, Texas, United States*

Heidi Clarke − *Department of Materials Science, Texas A&M University, College Station 77843-3003, Texas, United States*

Diane G. Sellers − *Department of Materials Science and Department of Chemistry, Texas A&M University, College Station 77843-3003, Texas, United States*

Erick J. Braham − *Department of Chemistry, Texas A&M University, College Station 77843-3255, Texas, United States*

Theodore E. G. Alivio − *Department of Chemistry, Texas A&M University, College Station 77843-3255, Texas, United States*

Sarbajit Banerjee − *Department of Materials Science and Department of Chemistry, Texas A&M University, College Station 77843-3003, Texas, United States;* orcid.org/0000-0002-2028-4675

Complete contact information is available at: https://pubs.acs.org/10.1021/acs.jpcc.0c04952

Notes

The authors declare no competing financial interest.

■ ACKNOWLEDGMENTS

We gratefully acknowledge the support from the President's Excellence Fund, Texas A&M University, through the X-Grants program for support of this research. A.Y. and E.J.B. gratefully acknowledge the support from the Data-Enabled Discovery and Design of Energy Materials (D3EM) program funded through the NSF award #1545403. S.B., D.G.S., and T.E.G.A. acknowledge the partial support from the NSF award #1809866 and from the Welch Foundation by award #A-1978-20190330.

■ REFERENCES

(1) Andrews, J. L.; Santos, D. A.; Meyyappan, M.; Williams, R. S.; Banerjee, S. Building Brain-Inspired Logic Circuits from Dynamically Switchable Transition-Metal Oxides. *Trends Chem.* **2019**, *1*, 711−726.

(2) Chen, L.; Wang, X.; Wan, D.; Cui, Y.; Liu, B.; Shi, S.; Luo, H.; Gao, Y. Energetics, electronic and optical properties of X (X = Si, Ge, Sn, Pb) doped VO2(M) from first-principles calculations. *J. Alloys Compd.* **2017**, *693*, 211−220.

(3) Du, J.; Gao, Y.; Luo, H.; Kang, L.; Zhang, Z.; Chen, Z.; Cao, C. Significant changes in phase-transition hysteresis for Ti-doped VO2 films prepared by polymer-assisted deposition. *Sol. Energy Mater. Sol. Cells* **2011**, *95*, 469−475.

(4) Béteille, F.; Morineau, R.; Livage, J.; Nagano, M. Switching properties of V1 − xTixO2 thin films deposited from alkoxides. *Mater. Res. Bull.* **1997**, *32*, 1109−1117.

(5) Patridge, C. J.; Whittaker, L.; Ravel, B.; Banerjee, S. Elucidating the Influence of Local Structure Perturbations on the Metal-Insulator Transitions of V1-xMoxO2 Nanowires: Mechanistic Insights from an X-ray Absorption Spectroscopy Study. *J. Phys. Chem. C* **2012**, *116*, 3728−3736.

(6) Miyazaki, K.; Shibuya, K.; Suzuki, M.; Wado, H.; Sawa, A. Correlation between thermal hysteresis width and broadening of metal−insulator transition in Cr- and Nb-doped VO_2 films. *Jpn. J. Appl. Phys.* **2014**, *53*, 071102.

(7) Wu, J.; Gu, Q.; Guiton, B. S.; De Leon, N. P.; Ouyang, L.; Park, H. Strain-Induced Self Organization of Metal−Insulator Domains in Single-Crystalline VO2Nanobeams. *Nano Lett.* **2006**, *6*, 2313−2317.

(8) Pouget, J. P.; Launois, H.; D'Haenens, J. P.; Merenda, P.; Rice, T. M. Electron Localization Induced by Uniaxial Stress in Pure VO2. *Phys. Rev. Lett.* **1975**, *35*, 873−875.

(9) Asayesh-Ardakani, H.; Yao, W.; Nie, A.; Marley, P. M.; Braham, E.; Klie, R. F.; Banerjee, S.; Shahbazian-Yassar, R. Direct evidence of M2 phase during the monoclinic-tetragonal (rutile) phase transition of W-doped VO2 nanowires. *Appl. Phys. Lett.* **2017**, *110*, 053107.
(10) Parija, A.; Waetzig, G. R.; Andrews, J. L.; Banerjee, S. Traversing Energy Landscapes Away from Equilibrium: Strategies for Accessing and Utilizing Metastable Phase Space. *J. Phys. Chem. C* **2018**, *122*, 25709−25728.
(11) Morin, F. J. Oxides which Show a Metal-to-Insulator Transition at the Neel Temperature. *Phys. Rev. Lett.* **1959**, *3*, 34.
(12) Kachi, S.; Kosuge, K.; Okinaka, H. Metal-Insulator Transition in V_nO_{2n-1}. *J. Solid State Chem.* **1973**, *6*, 258−270.
(13) Takahashi, I.; Hibino, M.; Kudo, T. Thermochromic properties of double-doped VO_2 thin films prepared by a wet coating method using polyvanadate-based sols containing W and Mo or W and Ti. *Jpn. J. Appl. Phys.* **2001**, *40*, 1391−1395.
(14) Verleur, H. W.; Barker, A. S.; Berglund, C. N. Optical Properties of VO2between 0.25 and 5 eV. *Phys. Rev.* **1968**, *172*, 788−798.
(15) Lee, S.; Hippalgaonkar, K.; Yang, F.; Hong, J.; Ko, C.; Suh, J.; Liu, K.; Wang, K.; Urban, J. J.; Zhang, X.; et al. Anomalously low electronic thermal conductivity in metallic vanadium dioxide. *Science* **2017**, *355*, 371−374.
(16) Oh, D.-W.; Ko, C.; Ramanathan, S.; Cahill, D. G. Thermal conductivity and dynamic heat capacity across the metal-insulator transition in thin film VO2. *Appl. Phys. Lett.* **2010**, *96*, 151906.
(17) Goodenough, J. B. The two components of the crystallographic transition in VO2. *J. Solid State Chem.* **1971**, *3*, 490−500.
(18) Zhou, Y.; Ramanathan, S. Mott Memory and Neuromorphic Devices. *Proc. IEEE* **2015**, *103*, 1289−1310.
(19) Okinaka, H.; Kosuge, K.; Kachi, S.; Nagasawa, K.; Bando, Y.; Takada, T. Electrical properties of V8O15 single crystal. *Phys. Lett. A* **1970**, *33*, 370−371.
(20) Cook, O. A. High-Temperature Heat Contents of V2O3, V2O4and V2O51. *J. Am. Chem. Soc.* **1947**, *69*, 331−333.
(21) Budai, J. D.; Hong, J.; Manley, M. E.; Specht, E. D.; Li, C. W.; Tischler, J. Z.; Abernathy, D. L.; Said, A. H.; Leu, B. M.; Boatner, L. A.; et al. Metallization of vanadium dioxide driven by large phonon entropy. *Nature* **2014**, *515*, 535−539.
(22) Vidas, L.; Günther, C. M.; Miller, T. A.; Pfau, B.; Perez-Salinas, D.; Martínez, E.; Schneider, M.; Gührs, E.; Gargiani, P.; Valvidares, M.; et al. Imaging Nanometer Phase Coexistence at Defects During the Insulator-Metal Phase Transformation in VO2 Thin Films by Resonant Soft X-ray Holography. *Nano Lett.* **2018**, *18*, 3449−3453.
(23) Clarke, H.; Carraway, B. D.; Sellers, D. G.; Braham, E. J.; Banerjee, S.; Arroyave, R.; Shamberger, P. J. Nucleation-controlled hysteresis in unstrained hydrothermal VO2 particles. *Phys. Rev. Mater* **2018**, *2*, 103402.
(24) Fan, W.; Cao, J.; Seidel, J.; Gu, Y.; Yim, J. W.; Barrett, C.; Yu, K. M.; Ji, J.; Ramesh, R.; Chen, L. Q.; Wu, J. Large kinetic asymmetry in the metal-insulator transition nucleated at localized and extended defects. *Phys. Rev. B: Condens. Matter Mater. Phys.* **2011**, *83*, 235102.
(25) Park, J. H.; Coy, J. M.; Kasirga, T. S.; Huang, C.; Fei, Z.; Hunter, S.; Cobden, D. H. Measurement of a solid-state triple point at the metal-insulator transition in VO2. *Nature* **2013**, *500*, 431−434.
(26) Wei, J.; Ji, H.; Guo, W.; Nevidomskyy, A. H.; Natelson, D. Hydrogen stabilization of metallic vanadium dioxide in single-crystal nanobeams. *Nat. Nanotechnol.* **2012**, *7*, 357−362.
(27) Shibuya, K.; Kawasaki, M.; Tokura, Y. Metal-insulator transition in epitaxial $V_{1-x}W_xO_2$ ($0 < x < 0.33$) thin films. *Appl. Phys. Lett.* **2010**, *96*, 022102.
(28) Alivio, T. E. G.; Sellers, D. G.; Asayesh-Ardakani, H.; Braham, E. J.; Horrocks, G. A.; Pelcher, K. E.; Villareal, R.; Zuin, L.; Shamberger, P. J.; Arróyave, R.; et al. Postsynthetic Route for Modifying the Metal-Insulator Transition of VO2 by Interstitial Dopant Incorporation. *Chem. Mater.* **2017**, *29*, 5401−5412.
(29) Filinchuk, Y.; Tumanov, N. A.; Ban, V.; Ji, H.; Wei, J.; Swift, M. W.; Nevidomskyy, A. H.; Natelson, D. In Situ Diffraction Study of Catalytic Hydrogenation of VO2: Stable Phases and Origins of Metallicity. *J. Am. Chem. Soc.* **2014**, *136*, 8100−8109.
(30) Booth, J. M.; Casey, P. S. Anisotropic structure deformation in the VO2 metal-insulator transition. *Phys. Rev. Lett.* **2009**, *103*, 086402.
(31) Zhang, J. J.; He, H. Y.; Xie, Y.; Pan, B. C. Boron-tuning transition temperature of vanadium dioxide from rutile to monoclinic phase. *J. Chem. Phys.* **2014**, *141*, 194707.
(32) Chen, Y.; Wang, Z.; Chen, S.; Ren, H.; Wang, L.; Zhang, G.; Lu, Y.; Jiang, J.; Zou, C.; Luo, Y. Non-catalytic hydrogenation of VO2 in acid solution. *Nat. Commun.* **2018**, *9*, 818.
(33) Sellers, D. G.; Braham, E. J.; Villarreal, R.; Zhang, B.; Parija, A.; Brown, T. D.; Alivio, T. E. G.; Clarke, H.; De Jesus, L. R.; Zuin, L.; et al. Atomic Hourglass and Thermometer Based on Diffusion of a Mobile Dopant in VO2. *J. Am. Chem. Soc.* **2020**, *142*, 15513.
(34) Asayesh-Ardakani, H.; Nie, A.; Marley, P. M.; Zhu, Y.; Phillips, P. J.; Singh, S.; Mashayek, F.; Sambandamurthy, G.; Low, K.-b.; Klie, R. F.; et al. Atomic Origins of Monoclinic-Tetragonal (Rutile) Phase Transition in Doped VO2 Nanowires. *Nano Lett.* **2015**, *15*, 7179−7188.
(35) Jones, A. C.; Berweger, S.; Wei, J.; Cobden, D.; Raschke, M. B. Nano-optical Investigations of the Metal−Insulator Phase Behavior of Individual VO2Microcrystals. *Nano Lett.* **2010**, *10*, 1574−1581.
(36) Braham, E. J.; Sellers, D.; Emmons, E.; Villarreal, R.; Asayesh-Ardakani, H.; Fleer, N. A.; Farley, K. E.; Shahbazian-Yassar, R.; Arroyave, R.; Shamberger, P. J.; Banerjee, S. Modulating the Hysteresis of an Electronic Transition: Launching Alternative Transformation Pathways in the Metal-Insulator Transition of Vanadium(IV) Oxide. *Chem. Mater.* **2018**, *30*, 214−224.
(37) Barker, A. S.; Verleur, H. W.; Guggenheim, H. J. Infrared Optical Properties of Vanadium Dioxide Above and Below the Transition Temperature. *Phys. Rev. Lett.* **1966**, *17*, 1286−1289.
(38) Dernier, P. D. Structural investigation of the metal-insulator transition in V6O13. *Mater. Res. Bull.* **1974**, *9*, 955−963.
(39) Wu, T.-L.; Whittaker, L.; Banerjee, S.; Sambandamurthy, G. Temperature and voltage driven tunable metal-insulator transition in individual $W_xV_{1-x}O_2$ nanowires. *Phys. Rev. B: Condens. Matter Mater. Phys.* **2011**, *83*, 073101.
(40) Chae, B. G.; Kim, H. T. Effects of W doping on the metal-insulator transition in vanadium dioxide film. *Phys. Rev. B: Condens. Matter Mater. Phys.* **2010**, *405*, 663−667.
(41) Gu, Q.; Falk, A.; Wu, J.; Ouyang, L.; Park, H. Current-Driven Phase Oscillation and Domain-Wall Propagation in WxV1-xO2Nanobeams. *Nano Lett.* **2007**, *7*, 363−366.
(42) Zhang, J.; He, H.; Xie, Y.; Pan, B. Theoretical study on the tungsten-induced reduction of transition temperature and the degradation of optical properties for VO_2. *J. Chem. Phys.* **2013**, *138*, 114705.
(43) Wu, T.-L.; Whittaker, L.; Banerjee, S.; Sambandamurthy, G. Temperature and voltage driven tunable metal-insulator transition in individual $W_xV_{1-x}O_2$ nanowires. *Phys. Rev. B: Condens. Matter Mater. Phys.* **2011**, *83*, 073101.
(44) Tselev, A.; Luk'yanchuk, I. A.; Ivanov, I. N.; Budai, J. D.; Tischler, J. Z.; Strelcov, E.; Kolmakov, A.; Kalinin, S. V. Symmetry Relationship and Strain-Induced Transitions between Insulating M1 and M2 and Metallic R phases of Vanadium Dioxide. *Nano Lett.* **2010**, *10*, 4409−4416.
(45) Cao, J.; Gu, Y.; Fan, W.; Chen, L. Q.; Ogletree, D. F.; Chen, K.; Tamura, N.; Kunz, M.; Barrett, C.; Seidel, J.; Wu, J. Extended Mapping and Exploration of the Vanadium Dioxide Stress-Temperature Phase Diagram. *Nano Lett.* **2010**, *10*, 2667−2673.
(46) Olson, G. B.; Tsuzaki, K.; Cohen, M. Statistical aspects of martensitic nucleation. *Mater. Res. Soc. Symp. Proc.* **1985**, *57*, 129−148.
(47) Chen, I.-W.; Chiao, Y.-H.; Tsuzaki, K. Statistics of martensitic nucleation. *Acta Metall.* **1985**, *33*, 1847−1859.
(48) Chen, I.-W.; Chiao, Y.-H. Theory and experiment of martensitic nucleation in ZrO2 containing ceramics and ferrous alloys. *Acta Metall.* **1985**, *33*, 1827−1845.

https://dx.doi.org/10.1021/acs.jpcc.0c04952
J. Phys. Chem. C 2020, 124, 21223−21231